International Forum on Aeroelasticity and Structural Dynamics
IFASD 2026
16-18 June 2026, Goettingen, Germany

HAP-ALPHA: DEVELOPMENT OF SYSTEM IDENTIFICATION MANOEUVRES FOR LOW-ALTITUDE FLIGHT TESTING OF A FLEXIBLE HIGH-ALTITUDE PLATFORM

Yasim J. Hasan[1], Arne Voß[2], Christian Raab[3], Nicolas Fezans[3]

[1]Institute of Flight Systems, DLR - German Aerospace Center
Lilienthalplatz 7, 38108 Braunschweig, Germany
yasim.hasan@dlr.de

[2]Institute of Aeroelasticity, DLR - German Aerospace Center
Bunsenstraße 10, 37073 Göttingen, Germany

[3]Institute of Flight Systems, DLR - German Aerospace Center
Lilienthalplatz 7, 38108 Braunschweig, Germany

Keywords: HAP-alpha, high-altitude platform, flight test manoeuvres, flight dynamics, aeroelasticity, loads, system identification

Abstract: This paper deals with the development of flight test manoeuvres that are defined for low-altitude flight testing of high-altitude platforms (HAP). Due to such aircraft's particularities, typical system identification manoeuvres are not always applicable and need to be adjusted. In addition, novel manoeuvres are defined. The results show that classical doublet manoeuvres are applicable when the time units are increased and/or comparatively strong control inputs are applied. A 13211-pitch manoeuvre is used instead of the better-known 3211 to limit airspeed excursions and a 121-bank input is used in lieu of a bank-to-bank manoeuvre. Frequency sweeps using aileron, stabiliser or rudder yield sufficient excitations of the structural modes and rudder doublets are the most critical with respect to loads. A final exemplary system identification test shows the general feasibility of the manoeuvres for obtaining adequate aircraft parameters. The work presented in this paper is conducted within the project *HAP-alpha*, in which the German Aerospace Center (DLR) is developing a flexible, solar-powered, fixed-wing HAP. In the project, an extensive low-altitude flight test campaign is planned, which will include dedicated test manoeuvres aimed at model validation and system identification.

NOMENCLATURE

Abbreviations

DLR	Deutsches Zentrum für Luft- und Raumfahrt (German Aerospace Center)
HAP	High-Altitude Platform
HTP	Horizontal tailplane
VTP	Vertical tailplane

Symbols

A	Amplitude
$\underline{\underline{A}}$, $\underline{\underline{B}}$, $\underline{\underline{C}}$, $\underline{\underline{D}}$	State-space matrices

$a_{i,j}$, $b_{i,j}$, $c_{i,j}$, $d_{i,j}$	Entries of the state-space matrices $\underline{\underline{A}}$, $\underline{\underline{B}}$, $\underline{\underline{C}}$ and $\underline{\underline{D}}$
c	Mean-aerodynamic chord
C_l	Rolling moment coefficient
C_L	Lift coefficient
C_{lX}	Derivative of rolling moment coefficient with respect to X
C_{LX}	Derivative of lift coefficient with respect to X
$C_{\eta X}$	Derivative of generalised force coefficient with respect to X
D	Damping ratio
$\vec{F}$	Force vector
g	Gravitational acceleration
$\underline{\underline{I}}$	Inertia tensor
i_{HTP}	Stabiliser deflection
$k_{\zeta,eff}$, $k_{\xi,eff}$	Rudder and aileron effectiveness factors
m	Mass
n_z	Vertical load factor
Ma	Mach number
$\vec{M}$	Moment vector
p, q, r	Rotational rates of roll, pitch and yaw
p^*, q^*, r^*	Non-dimensional rotational rates of roll, pitch and yaw
$\bar{q}$	Dynamic pressure
Q	Generalised force
res	Residual
S	Wing area
t	Time
u, v, w	Velocity components
$\vec{u}$	Input vector
$\vec{V}$	Velocity vector
V_{NE}	Never-exceed speed
$V_{\mathrm{O,max}}$	Maximum operating speed
$V_{\mathrm{O,min}}$	Minimum operating speed
V_{S}	Stall speed
V_{TAS}	True airspeed
$\vec{x}$	State vector
$\vec{y}$	Output vector
$\vec{z}$	Measurement vector
α	Angle of attack
β	Angle of sideslip
γ	Flightpath angle
η	Structural mode
$\varDelta$	Difference
$\varDelta t$	Base duration
ζ	Rudder deflection
$\hat{\xi}$	Combined aileron deflection
$\varPhi$, $\varTheta$, $\varPsi$	Euler angles, i.e. bank, pitch and heading
$\vec{\varOmega}$	Vector of rotational rates
ω_0	Natural frequency

Indices

A	Air-path value
Aero	Aerodynamics-related value
Flex	Flexibility-related value
Grav	Gravity-related value
K	Flight-path value
Prop	Propeller-related value
x, y, z	Value in direction of x, y or z

1 INTRODUCTION

HAP (high-altitude platform) aircraft are designed to operate in the lower stratosphere for a prolonged duration, often including multiple days or weeks of flight [1, 2]. This makes them suitable candidates for missions that typically lie in the field of satellite applications. General Earth observation missions in the civil [3] and military field, as well as telecommunications [4], are just two examples of their possible manifold use cases.

However, high-altitude long-endurance missions bring several challenges. The underlying aircraft needs a very high aerodynamic efficiency, ultralight structural weight and an extremely slow operating speed. Consequently, HAP aircraft are highly flexible and suffer from a significant susceptibility to wind disturbances. This is reflected by a number of mishaps involving HAP aircraft both at higher altitudes and at sea level [5–8]. Hence, these aircraft are, at present, primarily used as demonstration aircraft in the experimental context.

In order to pave the way for the operation of HAP aircraft on an ordinary and regular basis, a profound knowledge about their flight physics is indispensable. However, these aircraft operate on the verge of physical feasibility. Therefore, the applicability of common modelling approaches and assumptions are not always guaranteed and must be ascertained first. The most promising approach to tackle this issue is to perform flight testing. Using the recorded flight data, the underlying models are validated and can, if they are parameter-based, be improved via system identification. The resulting higher-accuracy models can subsequently be used for more significant analyses, the generation of improved flight control systems and for pilot-in-the-loop studies.

However, aircraft system identification requires the availability of flight test data of performed manoeuvres that adequately excite the aircraft's rigid-body and structural modes to a sufficient extent. Here, it is crucial that different influences can be subdivided to estimate the parameters correctly. The low-altitude flight physics of HAP aircraft pose a challenge here. As an example, a rudder doublet is typically used to excite the Dutch roll mode. After having stopped the control inputs, the aircraft continues to oscillate for a couple of seconds. Thereupon, it can be distinguished to which extent a generated yawing moment stems from rudder input, yaw rate, roll rate, angle of sideslip, etc. For fixed-wing HAP aircraft, however, the rigid-body modes [9] and even lower-order aeroelastic modes [10] can be overcritically, or at least strongly, damped at low altitudes. As a result, after reducing the control inputs, the aircraft returns relatively fast to a rather steady flight condition. Hence, distinguishing between different influencing factors becomes significantly more challenging. Therefore, a larger amount of rudder input would be desirable. However, at the same time, it must be ensured that the associated limiting load cases are not exceeded. In addition, the typical flight envelope of HAP aircraft comprises a rather narrow airspeed band which must not be left either. Both of these safety-related aspects limit the allowable amount of control inputs again. Therefore, the applicability of classical system identification manoeuvres is limited. Instead, such manoeuvres must be specifically tailored to the aircraft's particularities and need to account for the above-listed limits and challenges.

DLR (German Aerospace Center) is currently developing a solar-driven fixed-wing high-altitude platform in the project *HAP-alpha*. The aircraft was initially intended and designed to perform 30-days-long non-stop missions in the lower stratosphere while carrying interchangeable payload of 5 kg [11]. A comprehensive flight test campaign is planned for summer 2026, within which low-altitude flight test manoeuvres are needed for model validation and system identification. The manoeuvres developed and described in this paper will be performed in the context of this flight test campaign.

This paper deals with the development of system identification manoeuvres for flexible fixed-wing HAP and investigates which flight manoeuvres are adequate to perform system identification for such aircraft. For this purpose, it uses time simulations from a flight dynamics model (section 3, section 4) that accounts for influences of the flight shape-dependent aerodynamic changes and the structural dynamics. Subsequently, these manoeuvres are analysed using a dynamic aeroelasticity analysis to assess the associated loads and to limit control inputs (section 5). Finally, surrogate flight test data are generated by simulating the manoeuvres with the flight dynamics model including low-magnitude wind. Using these data, an exemplary system identification test is performed using simulated surrogate flight test data to assess the manoeuvres' suitability for system identification (section 6).

2 THE DLR HAP AIRCRAFT

The works described in this paper were performed using the DLR HAP-alpha aircraft. It is a flexible, solar-powered fixed wing HAP that was developed in the context of the DLR-project *HAP-alpha*. This section presents the aircraft.

2.1 The Aircraft

Figure 1 shows a sketch of the DLR HAP-alpha aircraft. It has a wing with high aspect ratio, a span of 27 m, an area of 36 m^2, and outer wing sections with 12° dihedral, as well as a payload compartment located inside the aircraft nose. The aircraft has two electrically-driven propellers. Its total mass is around 136 kg. Asymmetrically deflected ailerons and a rudder are used to generate lateral-directional control moments. For longitudinal motion, a fully movable horizontal tailplane is used. As such, it resembles a typical stabiliser of conventional aircraft. Therefore, it is termed "stabiliser" in this work even though it is, besides trimming, also used as an elevator.

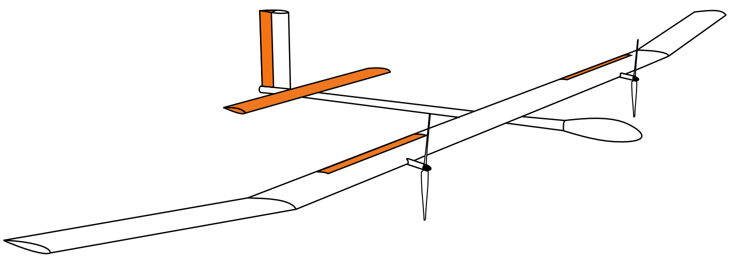

Figure 1: Sketch of the DLR HAP-alpha aircraft with control surfaces highlighted in orange [9]

2.2 Flight Envelope

As already stated, the very narrow speed band of the aircraft poses a significant challenge when it comes to system identification manoeuvres, particularly in longitudinal direction. Table 4 shows the flight envelope at sea level. It consists of an outer envelope and an inner envelope. The outer envelope is defined by stall speed V_{S} and the never-exceed speed V_{NE}. It must never be left because otherwise an uncontrollable flight condition or structural damage might occur.

Table 4: Speed envelope of the aircraft at sea level

Stall speed V_{S}	**Minimum operating speed** $V_{\mathrm{O,min}}$	**Maximum operating speed** $V_{\mathrm{O,max}}$	**Never-exceed speed** V_{NE}
6.5 m/s	9.1 m/s	11.0 m/s	14.5 m/s

The inner envelope is the operation envelope, which is defined by the minimum operating speed $V_{\mathrm{O,min}}$ and the maximum operating speed $V_{\mathrm{O,max}}$. During nominal flight, the aircraft is supposed to stay within this envelope. Excursions are only allowed when externally triggered, for instance due to gust encounters. As soon as the aircraft leaves this inner envelope, commands need to be applied such that the aircraft returns to this envelope promptly. During flight test manoeuvres, the aircraft should preferably remain inside this envelope. If leaving this inner envelope is unavoidable, this should be as short as possible and the values should not significantly over- or undershoot the limit values.

2.3 Structural Modes

The DLR HAP-alpha is an extreme lightweight aircraft with a high aspect ratio. Consequently, it has a high degree of structural flexibility. Figure 2 exemplarily depicts the first two structural modes of the aircraft with lowest frequency. These have been obtained after a model update based on a ground vibration test [12]. As shown, the first mode is a symmetric wing bending and the second mode is an asymmetric wing in-plane mode. The corresponding frequencies are low compared to those of typical passenger aircraft. As a result, they are likely to interfere with the rigid-body modes to a larger extent, which has to be taken into account when designing system identification manoeuvres.

2.4 Flight Test Instrumentation

The flight test manoeuvres developed in this paper will be performed within the flight test campaign of *HAP-alpha*. For this reason, the flight test instrumentation of the underlying aircraft is briefly presented here. Even though the instruments are not used in the context of the system identification test later in this paper, they give an idea about which quantities will be measured during the flight test and thus need to be sufficiently excited. Therefore, the developed manoeuvres are strongly linked to the availability of different instruments and can only be understood to the fullest against this background.

The aircraft is equipped with some instruments that provide the typical set of measurements of rigid-body flight quantities. This includes an inertial measurement unit located approximately 2 m in front of the centre gravity, which provides accelerations and rotational rates, and, after

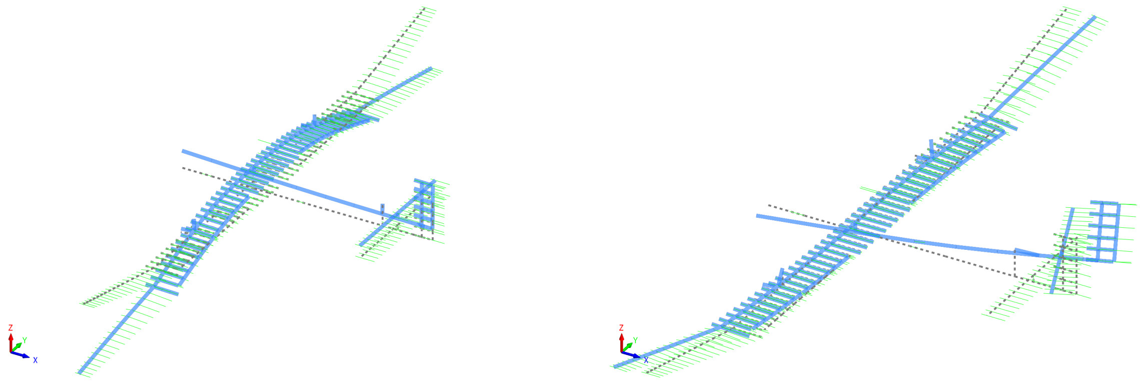

(a) Mode 1, symmetric wing bending, 0.99 Hz

(b) Mode 2, wing in-plane, scissor mode, 1.37 Hz

Figure 2: First and second structural modes after model update based on ground vibration test [12]

integration, velocities and Euler angles. Static and total pressure, airspeed and aerodynamic angles are measured by a five-hole-probe. It is integrated into a boom, which is installed at the wing leading edge approximately 4 m right of the aircraft centre line.

In addition to the instruments dedicated to measuring rigid-body quantities, several accelerometers and strain gauges are included into the aircraft structure. Figure 3 shows the respective positions of all accelerometers (red dots), strain gauges (green lines) and additional temperature sensors (blue dots). While all accelerometers are, in principle, capable of measuring rotations around and accelerations along the three body axes, only the more relevant signals are used to reduce the amount of data. The sensors are supposed to measure the elastic response of the aircraft while the strain gauges are additionally needed to estimate sectional loads. For this reason, the flight test manoeuvres developed in this paper are not only expected to sufficiently excite the rigid-body dynamics but also to cause larger deformations and loads. More information about the aeroelasticity-related flight test instrumentation of the aircraft can be found in [13].

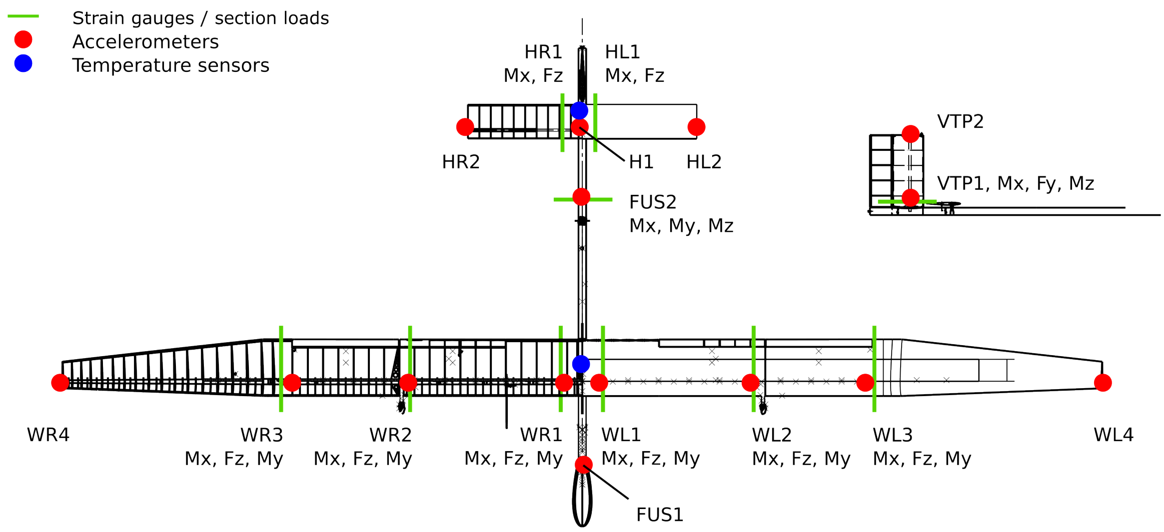

Figure 3: Distribution of sensors for determination of structural deformations and loads [13]

3 FLIGHT DYNAMICS MODEL FOR FLEXIBLE AIRCRAFT

The initial design of all test manoeuvres has been made by first simulating common manoeuvres with a flight dynamics model that accounts for aircraft flexibility and adjusting them according to the time response. This section presents this model. It has, in most parts, already been described in previous works [9, 10, 14]. Therefore, only an overview is provided here. The rigid-body equations of motion are given by

$$\begin{aligned}\dot{\vec{V}}_{\mathrm{K}} &= -\vec{\Omega}_{\mathrm{K}} \times \vec{V}_{\mathrm{K}} + \frac{1}{m}\left(\vec{F}_{\mathrm{Prop}} + \vec{F}_{\mathrm{Grav}} + \vec{F}_{\mathrm{Aero}} + \vec{F}_{\mathrm{Flex}}\right),\\ \dot{\vec{\Omega}}_{\mathrm{K}} &= \underline{\underline{I}}^{-1}\left(-\vec{\Omega}_{\mathrm{K}} \times (\underline{\underline{I}}\vec{\Omega}_{\mathrm{K}}) + \vec{M}_{\mathrm{Prop}} + \vec{M}_{\mathrm{Aero}} + \vec{M}_{\mathrm{Flex}}\right),\end{aligned} \tag{1}$$

where index K denotes that the values are the flight-path-related quantities. Here, $\vec{V}$ is the velocity vector, $\vec{\Omega}$ is the vector of the rotational rates p, q and r, $\underline{\underline{I}}$ is the inertia tensor, $\vec{F}$ represents the force vector, and $\vec{M}$ the moment vector. The structural dynamics is included via the modes. The associated structural equations of motion read

$$\ddot{\eta}_i + 2D_i\,\omega_{0,i}\,\dot{\eta}_i + \omega_{0,i}^2\,\eta_i = \frac{Q_i}{m_i}. \tag{2}$$

Here, D_i is the damping, $\omega_{0,i}$ is the natural frequency and Q_i is the generalised force of the respective mode. The mode deflections η_i are defined with respect to the current flight shape, i.e. the steady aircraft deformation due to the acting forces in a horizontal $1g$-flight at a specific airspeed. The coupling between rigid-body motion and structural modes is realised as proposed by Waszak and Schmidt [15] via the aerodynamic forces. Therefore, Eq. 1 includes the forces due to the structural modes (denoted "Flex"). These are obtained by assuming quasi-steady aerodynamics and considering influences due to the structural mode deflections and rates. Including the first 15 flexible modes η_i with the lowest frequencies, this yields, exemplarily shown for the lift coefficient,

$$C_L = \sum_{j=1}^{15} C_{L\eta_{j_{\mathrm{b}}}}\eta_j + \sum_{j=1}^{15} C_{L\dot{\eta}_{j_{\mathrm{b}}}}\frac{\dot{\eta}_j\,c}{2V_{\mathrm{TAS}}}, \tag{3}$$

where c is the mean aerodynamic chord. In return, the generalised forces Q_i in Eq. 2 include influences due to flexible modes and due to rigid-body flight quantities:

$$\begin{aligned}Q_i = \bar{q}Sc\Bigg(&C_{\eta_i u}\,\Delta u_{\mathrm{A}} + C_{\eta_i v}\,v_{\mathrm{A}} + C_{\eta_i w}\,\Delta w_{\mathrm{A}} + C_{\eta_i p}\,p^* + C_{\eta_i q}\,q^* + C_{\eta_i r}\,r^* + C_{\eta_i \xi}\,\hat{\xi}\\ &+ C_{\eta_i i_{\mathrm{HTP}}}\,\Delta i_{\mathrm{HTP}} + C_{\eta_i \zeta}\,\zeta + C_{\eta_i F_{\mathrm{Prop}}}\,\Delta F_{\mathrm{Prop}} + \sum_{j=1}^{15} C_{\eta_i \eta_j}\,\eta_j + \sum_{j=1}^{15} C_{\eta_i \dot{\eta}_j}\,\frac{\dot{\eta}_j c}{2\,V_{\mathrm{TAS}}}\Bigg).\end{aligned} \tag{4}$$

Here, $\bar{q}$ is the dynamic pressure, S is the wing area, c the mean aerodynamic chord, u_{A}, v_{A}, w_{A} are the velocity components with respect to the flow, $\hat{\xi}$ is the combined aileron deflection, i_{HTP} is the stabiliser deflection where HTP denotes horizontal tailplane, ζ is the rudder deflection and F_{Prop} is the propeller-induced thrust force. Note here that, in accordance with the fact that the structural mode deflections are defined about the flight shapes, some quantities are included as differences (denoted with a Δ). These represent the differences with respect to the required deflections for a steady-state $1g$ flight, for which the corresponding flight shape is given. The rigid-body aerodynamic coefficients are also given in the form of derivatives. Exemplarily shown for the rolling moment coefficient, this yields

$$C_l = C_{l\beta}\,\beta + C_{lp}\,p^* + C_{lr}\,r^* + C_{l\xi}\,\hat{\xi}\cdot k_{\xi,eff} + C_{l\zeta}\,\zeta\,k_{\zeta,eff}, \tag{5}$$

where $k_{\xi,eff}$ and $k_{\zeta,eff}$ are factors that account for elastic aileron and rudder effectiveness. All derivatives included in the model are given in dependency of the flight shapes. In order to obtain the values corresponding to the current flight shape, an interpolation over the equivalent airspeed is performed. This way, airspeed excursions, in principle, affect both the structural modes (e.g. $C_{\eta_i u}\,\Delta u_{\mathrm{A}}$ in Eq. (4)) and the flight shapes (through interpolation of derivatives) and are therefore, in principle, represented twice. In order to cope with this issue and not doubly include the influence, a frequency blending is performed with a cutoff frequency of 0.5 Hz. Here, the low frequency portion of the airspeed is used to apply flight-shape changes and the high frequency portion excites the modes about the flight shapes [10]. In order to account for lag effects, forces are considered independently at main wing, HTP and vertical tailplane (VTP). Furthermore, stall is modelled at the main wing and VTP [14].

4 DEVELOPMENT OF SYSTEM IDENTIFICATION MANOEUVRES

This section describes the system identification manoeuvres developed in the context of this work for low-altitude flight testing of the DLR HAP-alpha aircraft. The development was done in an iterative process, in which the manoeuvres were simulated, starting with typical test manoeuvres. In the following, the manoeuvres were successively adjusted until they were deemed adequate in terms of the aircraft response. Afterwards, a clearance with respect to the associated loads was performed.

4.1 Requirements for Adequate Manoeuvres

Numerous prior works have focused on the design of system identification manoeuvres, cf. [16–18] and references therein. Many of the prior works also aimed at optimising the manoeuvres, usually with the aim of reducing the uncertainty bounds on the estimated parameters or reducing the flight test time, see for example [19–23]. These works typically yield complex manoeuvres, which do have adequate properties for system identification, but often require to be performed via computerised inputs and were not considering very tight flight and loads envelopes.

The characteristics of the present vehicle and its flight envelope shifts a bit the focus away from strong identifiability and the following hard requirements were defined:

- **Limitation of loads:** While some amount of flexible mode excitation and loads is desirable for comparisons of simulation results and flight tests, these should not be excessive as modelling and manufacturing uncertainties may be present. Remaining within 50 % of the target load envelope, which represents the loads that the aircraft was sized with, was defined as an acceptable maximum. Complex manoeuvres exciting many modes at the same time could yield very different peak load levels when considering uncertainties, for example in mode frequencies and damping. Such complex manoeuvres should be avoided, at least during the initial model validation.
- **Remain within the flight envelope:** The allowable speed band is very narrow. Excess airspeed deviations thus directly increase the risk of a loss of aircraft. The manoeuvres must be defined such that the aircraft will not come close to or exceed the limits of the outer flight envelope (i.e. $V_{\mathrm{TAS}} > V_{\mathrm{S}}$ or $V_{\mathrm{TAS}} < V_{\mathrm{NE}}$).

The objectives (soft requirements) for the design of the manoeuvres are defined as follows:

- **Sufficient and distinct excitations of the quantities of interest:** To facilitate the identification process, the different desired flight quantities (e.g. angle of attack, yaw rate, etc.) should be notably excited for a sufficient amount of time. In addition, a separation of the excitations of different quantities is to be sought and preferred.
- **Small airspeed excursions:** The airspeed has a strong influence on the flight shapes and thereby on the aerodynamic characteristics. Therefore, larger deviations would complicate the subsequent identification process, as the derivatives vary more strongly over a single manoeuvre. The risk of small short-term excursions of the operation flight envelope (i.e. $V_{\mathrm{TAS}} < V_{\mathrm{O,min}}$ or $V_{\mathrm{TAS}} > V_{\mathrm{O,max}}$) should be as low as possible.
- **Easy to perform by a human pilot:** In the framework of the *HAP-alpha* flight tests, the flight control system is planned to be used to execute the pre-defined system identification manoeuvres. Still for maximum flexibility and as a fall-back solution, it was desired to define manoeuvres which are already validated in terms of loads and airspeed excursions and which could still easily be flown manually, if needed. Consequently, manoeuvres which could be performed by a human pilot are preferred, which eliminates more complex signals such as multi-sines e.g. [24] or wavelet-based multi-axis signals e.g. [25].

The following sections present the manoeuvres that were found to be most adequate. The manoeuvres involving stabiliser deflections are shown first, followed by roll and then yaw manoeuvres. In addition, frequency sweeps are shown. In order to limit the occurring accelerations, a maximum control surface deflection rate of 30 °/s is applied for all manoeuvres.

4.2 Stabiliser 13211 and Stabiliser Doublet

Manoeuvres with stabiliser, respectively elevator, inputs are commonly used to excite the short period and the phugoid modes. Single-step or multistep inputs are quite commonly used for this. Such manoeuvres are described by a few parameters: typically the duration and amplitude of each step. In the case of multistep manoeuvres, the duration of the successive steps follow a specific pattern and two parameters are then sufficient: the amplitude A and a base duration Δt.

By varying Δt, the whole spectrum of the excitation can be shifted in frequency. The frequencies of the eigenmodes of interest are usually targeted by choosing the appropriate value for Δt [17, 25]. Multistep signals with different durations can be used to spread out the excitation in the frequency domain such that the excitation signal works robustly for a wider range of frequencies and thereby system behaviours. These difference in behaviour may results from modelling or manufacturing uncertainties, different masses or mass distributions (not relevant for HAP-alpha), or flight conditions. At low altitudes, the short period mode of HAP-alpha is overcritically damped and, instead, exhibits two strongly decaying aperiodic modes [9, 10]. For this reason, the usual derivation of the base duration Δt as a function of the short period frequency is not applicable, but the principle remains valid. In this work, the amplitude and base duration were varied in simulation until the time response of that aircraft was deemed acceptable.

The two selected manoeuvres are multistep manoeuvres: a 13211 and a doublet. The 13211 manoeuvre is a variation of the well-known 3211-manoeuvre [16, 26]. The original 3211 manoeuvre is illustrated in Figure 4a (blue line) and consists of four consecutive steps of the same magnitude but with alternating direction with durations of $3\,\Delta t$, $2\,\Delta t$, $1\,\Delta t$, and $1\,\Delta t$, respectively. As pointed out in [27–29], it is one of the most common longitudinal input signals used in system identification, probably because it is effective and very easy to use. With the longer step at the beginning of the manoeuvre, the aircraft starts deviating in altitude and speed early during the manoeuvre and the sum of all control actions is also non-zero such that the aircraft tends to execute most of the manoeuvre at a slightly different speed and to leave the current flight point. This tendency can be reduced in different ways. By flipping the 3-2-1-1 signal, e.g. it becomes a 1-1-2-3 signal which excites the higher frequencies first and limits this effect [17,30]. A modified amplitude can also be applied to each step to compensate the differences in duration, for example by using steps of amplitude 0.8 A, -1.2 A, 1.1 A, and -1.1 A (with nominal amplitude A) as mentioned in [17] and illustrated in orange in Figure 4a. In practice, such fine adjustments of the step amplitude are not easy to do for human pilots, so adding a step of duration 1 Δt at the start of the manoeuvre provides an easier way to obtain a similar effect (cf. Figure 4b).

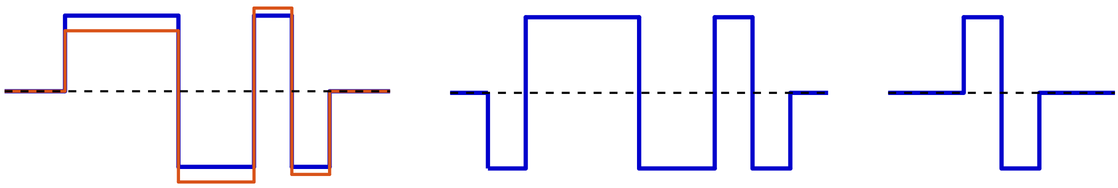

(a) original 3-2-1-1 input signal (blue: with equal amplitudes, orange: with modified amplitudes)

(b) 1-3-2-1-1 input signal

(c) doublet input signal

Figure 4: Typical multistep input signals

Two variations of the 13211-manoeuvres were selected and are shown in Figure 5a along with the simulated flight dynamics model response without wind. These are a longer manoeuvre (blue solid lines) with a base duration of 1 s and deflections of $\pm 2°$ relative to the trim setting and a shorter one (red dashed lines) with a base duration of 0.5 s but stronger inputs of $\pm 5°$. The first allows keeping a modified angle of attack for a longer duration whereas the second allows reaching higher pitching rates q and accelerations $\dot{q}$. In both cases, the airspeed variation remains within about ± 1 m/s, and reaches $V_{\mathrm{O,min}}$ but does not significantly fall below this speed.

In addition, a stabiliser doublet (Figure 4c, Figure 5b) with a time unit of 1 s and a deflection of 10° is also selected. It allows reaching stronger vertical load factors and structural deflections (shown in Figure 5b for the first symmetric wing bending structural mode η_1), which is required for the validation of the aeroelastic model. Second, this manoeuvre excites the phugoid mode well, as can be seen by the oscillations of airspeed V_{TAS} and the flight path angle γ after the stabiliser input is removed after 3 s. Note that the HAP-alpha's phugoid mode has a comparatively strong damping ratio and a high frequency due to its small weight and airspeed [9, 10].

All manoeuvres are to be performed in both directions, hence with first input down, respectively up. In Figure 5, only the manoeuvres with initial downwards command, i.e. positive stabiliser deflection are shown. Figure 10 will later show the opposite manoeuvres in the context of the loads analysis.

4.3 Aileron 121 and Aileron Sine

Next, the aileron manoeuvres are presented. Typically, bank-to-bank manoeuvres are performed using ailerons and, if applicable, spoilers to a certain extent to achieve larger roll rates and to set up high bank angles, while at the same time keeping the yawing motion to a possible minimum. This allows to identify the rolling-motion-related parameters. In case of HAP-alpha, such an approach is not possible as the achievable roll rates are extremely low due to the high-aspect-

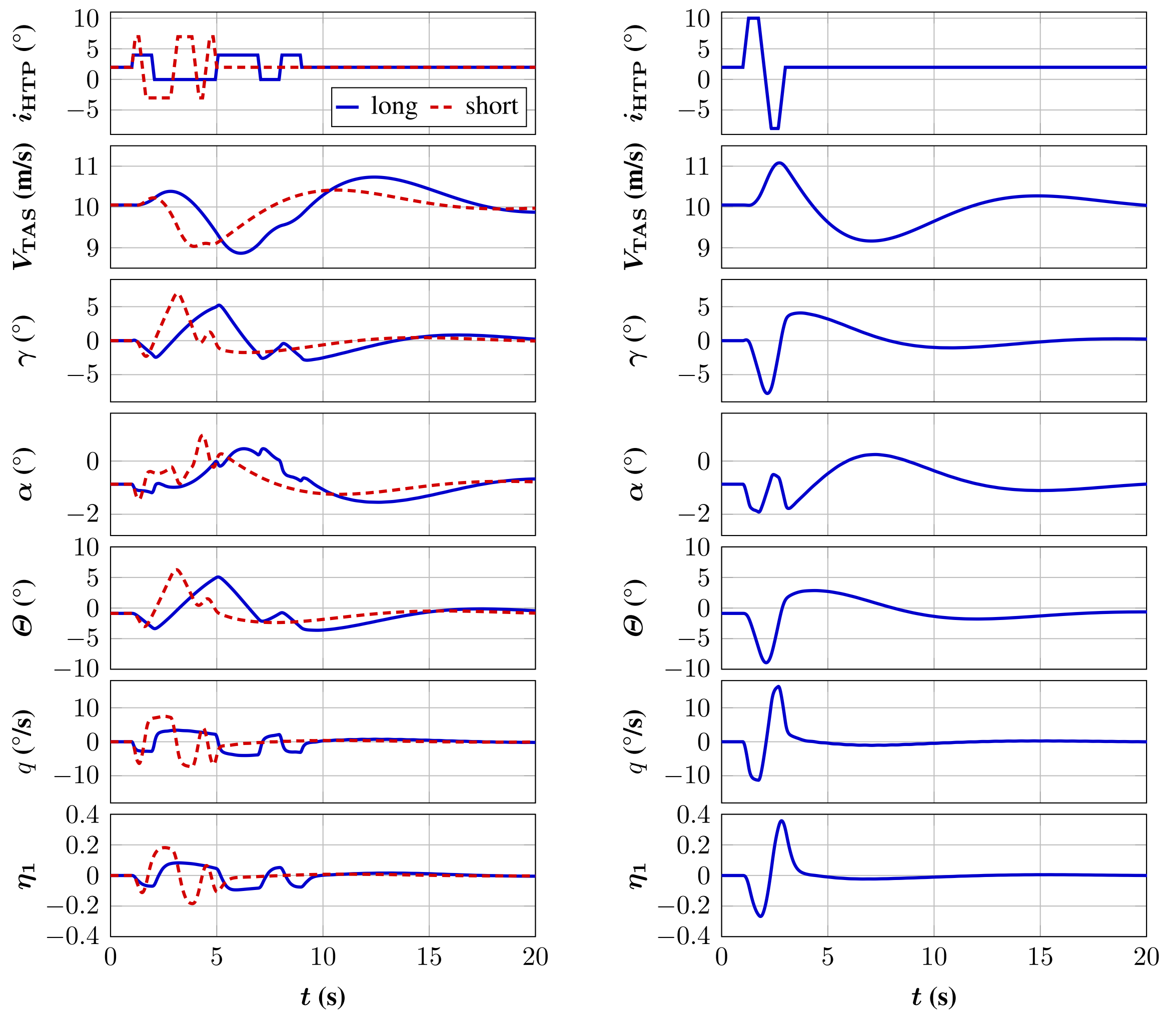

(a) Stabiliser 13211, first down

(b) Stabiliser doublet, first down

Figure 5: Time histories for vertical manoeuvres performed with flight dynamics model

ratio wing and a very small aileron effectiveness. In addition, the allowed bank angle is limited due to the risk of entering a spiral descent. In order to cope with these issues, a different manoeuvre is envisaged as the primary system identification roll manoeuvre. It is a so-called 121-manoeuvre. Hence, the first step is to one side with a base duration of 1 Δt, followed by a step to the other side with 2 Δt and a final step to the first side again with 1 Δt. Figure 6 shows the aileron manoeuvres and depicts the 121-manoeuvre in Figure 6a. In the flight test, all manoeuvres are performed to both sides. While, in theory, both yield equivalent results, this serves to identify unintentional asymmetries of the aircraft and also allows a plausibility check. Here, only the manoeuvres that start with a left input are shown.

As shown, a base duration Δt of 5 s is used together with a strong aileron input of 10°. This yields maximum roll rates p of approximately ±2°/s, which is a comparatively high value for the aircraft. Accordingly, bank angles of $\Phi = \pm 5°$ are achieved. As a reference, above a bank angle of approximately ±7° in turning flight, local stall is likely to occur at the inner-turning wing at sea level for HAP-alpha. Therefore, it can be concluded that this manoeuvre already leads to sufficient excursions even though for conventional aircraft these values would be very low.

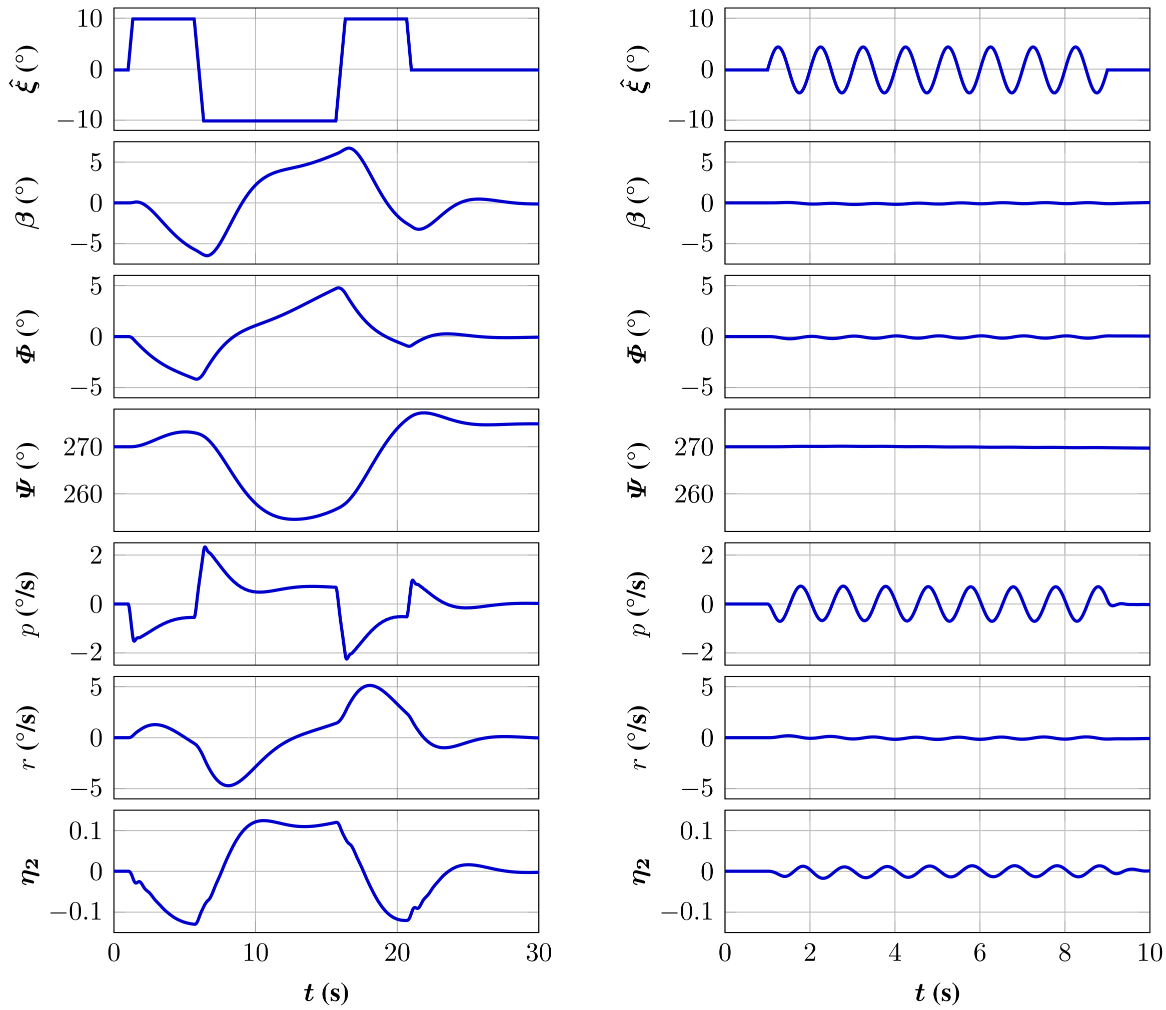

(a) Aileron 121, first left

(b) Aileron sine, first left

Figure 6: Time histories for roll manoeuvres performed with flight dynamics model

However, the time histories also show that the aircraft has a very strong roll-yaw coupling. This is particularly visible in the yaw rate r, which reaches higher values than the roll rate p in this manoeuvre and the sideslip angle β, whose values and trends are similar to those of the bank angle Φ. This can pose a difficulty when estimating the parameters as it hinders a clear subdivision of the according effects. For this reason, an additional manoeuvre is added, whose time histories are depicted by Figure 6b. It is an aileron sine input. A frequency of 1 Hz is used, which is still well below the first asymmetric mode η_2 (cf. Figure 2b). Accordingly, as it can be seen, this mode is not resonant for the given inputs and only reaches comparatively small values. On the other hand, the input frequency is high enough to prevent the sideslip angle β from reaching larger values. The yaw rate is also small, while the roll rate at least reaches values up to ± 1°/s.

4.4 Rudder Doublet

In this section, the rudder manoeuvres are presented. Typically, rudder inputs are used to excite the Dutch roll mode. However, similar to the short period mode, the HAP-alpha's Dutch roll mode is strongly damped and barely oscillates [9, 10]. For this reason, a signal sizing based on the Dutch roll's characteristics is again not reasonable. Instead, the inputs must be designed in such a way that the direct responses to the control inputs are distinct. Rudder doublets are used in two different variants, as shown in Figure 7.

The first variant is a longer manoeuvre with a base duration Δt of 5 s and a magnitude of 5° (blue solid lines). As shown, after the inputs are completed, the aircraft returns fast to a steady state which indicates that the Dutch roll decays fast. With this longer manoeuvre, a larger sideslip angle β establishes over time. After the rudder is set back to zero, there is a small overshoot visible in all quantities. In addition, a short manoeuvre with a base duration Δt of 1 s is used (red dashed lines). In return, a large rudder input of 10° is used. This manoeuvre is added to achieve larger yaw rates r that are still existent for a larger time span after the rudder input has been set back to zero.

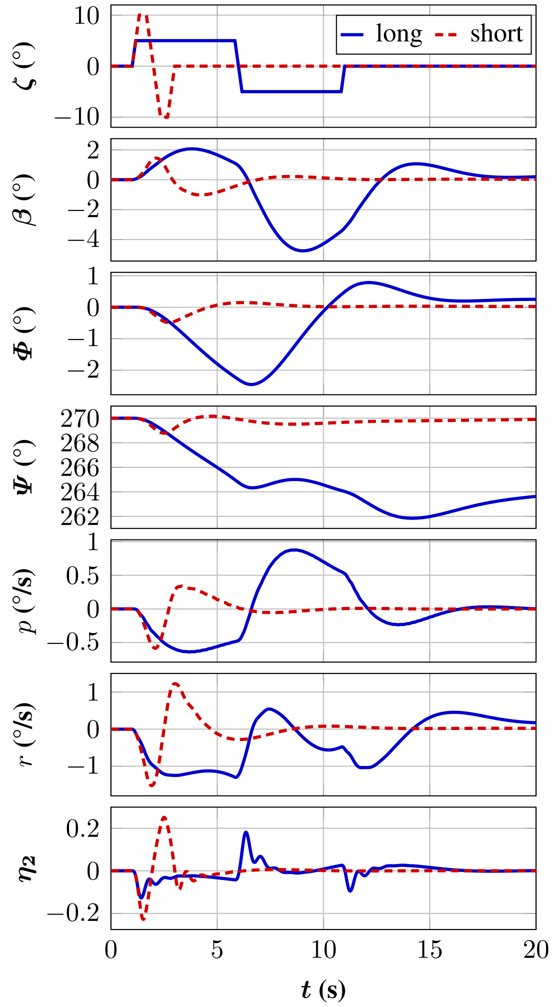

Figure 7: Time histories for rudder doublets (first left) performed with flight dynamics model

The approach of dividing the manoeuvre into two variants in order to achieve either higher sideslip angles or higher yaw rates is similar to that performed for the stabiliser inputs. However, here the driver is not the airspeed excursion. Instead, applying larger inputs for a longer time span is limited by the associated vertical-tail loads, as a strong rudder deflection with a larger sideslip angle of the same direction is a critical load case.

4.5 Frequency Sweeps

Finally, frequency sweeps are chosen to excite a broader frequency range. It will be performed separately using stabiliser, ailerons and rudder. This manoeuvre is characterised by a sinusoidal signal, which starts at a rather low frequency. Over time, the frequency is gradually increased. Even though such manoeuvres are more common in the context of frequency domain applications, experiments have shown that such manoeuvres are well applicable in flight testing to excite the structural dynamics [31, 32]. Frequency sweeps are very powerful and relatively easy to perform manually, but tend to require longer duration than many other methods [33]. Figure 8 exemplarily shows the time history responses due to a stabiliser frequency input.

For HAP-alpha, the frequency is varied from 0.2 Hz to 10.0 Hz to excite a high number of structural modes. In order to not exceed the afore-mentioned control input limit of 30°/s at high frequencies, the deflection magnitude is limited to 1°. As shown by Figure 8, the rigid-body flight quantities remain close to the initial flight condition. The airspeed V_{TAS} deviates only by

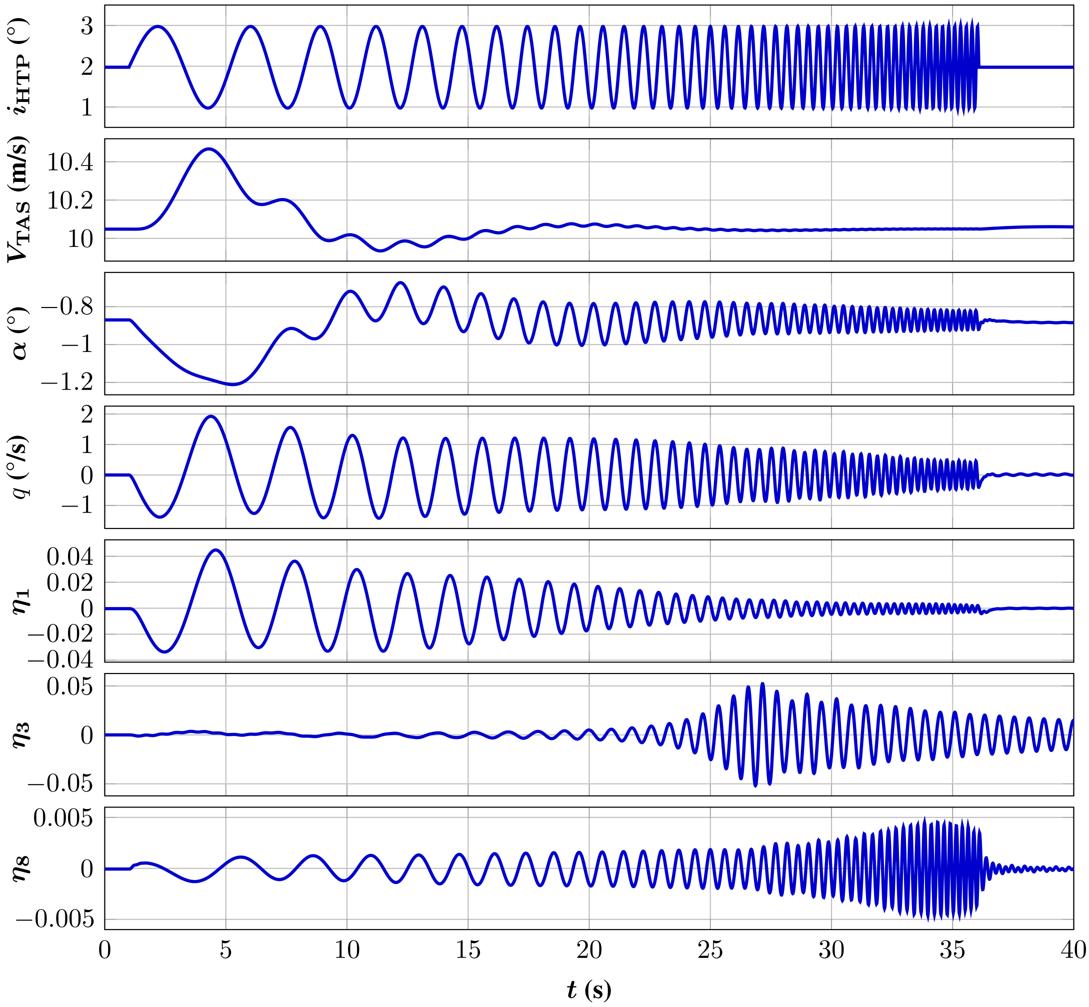

Figure 8: Time histories for stabiliser frequency sweep performed with flight dynamics model

around 0.5 m/s and the angle of attack α only responds to the first oscillation to a larger extent. The corresponding pitch rate q is also comparatively low. In the bottom three plots of Figure 8, the structural modes 1, 3 and 8 are shown, which are the symmetrical modes with lowest frequency. Even though the asymmetrical modes are also excited by this longitudinal manoeuvre due to the modes' cross-coupling, the time histories of these modes are more interesting. Mode 3 is a symmetrical wing in-plane mode and mode 8 is a wing bending with fuselage bending. Both are not shown in this paper but more information and plots are provided by [12]. As shown, all modes are well excited by the stabiliser frequency sweep and resonances are visible for mode 3 and 8.

4.6 Summary of Manoeuvres

Finally, this section summarises the manoeuvres that were developed for low-altitude flight testing of HAP-alpha and have been shown in the previous sections. For this purpose, Table 5 lists them and provides the respective parameters. Recall that all manoeuvres are performed in both directions even though for the lateral-directional manoeuvres symmetry is expected. Please note that not only the above-described manoeuvres will be used for system identification. All other flight data without dedicated manoeuvres might also be used. This involves particularly turns, take-offs and landings. In addition, some more manoeuvres that are not specifically designed for the HAP-alpha might be included on demand. These are thrust step inputs and doublets, as well as steady-heading sideslip manoeuvres.

Table 5: Summary of all low-altitude system identification manoeuvres

Control surface	Manoeuvre	Base duration/ frequency	Magnitude	Direction
Stabiliser	13211, long	1.0 s	2.0°	First up
	13211, long	1.0 s	2.0°	First down
	13211, short	0.5 s	5.0°	First up
	13211, short	0.5 s	5.0°	First down
	Doublet	1.0 s	10.0°	First up
	Doublet	1.0 s	10.0°	First down
	Frequency sweep	0.2 Hz – 10.0 Hz	1.0°	First up
	Frequency sweep	0.2 Hz – 10.0 Hz	1.0°	First down
Ailerons	121	5.0 s	10.0°	First left
	121	5.0 s	10.0°	First right
	Sine	1.0 Hz	4.5°	First left
	Sine	1.0 Hz	4.5°	First right
	Frequency sweep	0.2 Hz – 10 Hz	1.0°	First left
	Frequency sweep	0.2 Hz – 10 Hz	1.0°	First right
Rudder	Doublet, long	5.0 s	5.0°	First left
	Doublet, long	5.0 s	5.0°	First right
	Doublet, short	1.0 s	10.0°	First left
	Doublet, short	1.0 s	10.0°	First right
	Frequency sweep	0.2 Hz – 10.0 Hz	1.0°	First left
	Frequency sweep	0.2 Hz – 10.0 Hz	1.0°	First right

5 LOADS AND AEROELASTIC ANALYSIS

As described in section 2, the aircraft is highly elastic and many design aspects are driven by loads and aeroelasticity and even involve active load alleviation techniques [34]. The aeroelastic modelling comprises individual models for aerodynamics, mass, stiffness and the flight controller, coupled in the aeroelastic simulation software Loads Kernel [35, 36]. The numerical simulation models are described in detail in previous publications [37–39] while this section focuses on the validation. For example, the aerodynamic panels methods, vortex lattice (VLM) and doublet lattice method (DLM) [40, 41], are fully applicable due to the slow flight speed leading to a low Mach number ($\mathrm{Ma} < 0.3$) and the authors are confident in the aerodynamic modelling as long as the geometry and airfoils are correct. In addition, results were compared against higher fidelity simulations from the aerodynamic design team and showed a good agreement. The mass model was checked by weighting all structural components and systems, leading to a very close match with the total mass (residual $\mathrm{res} < 200\,\mathrm{g}$) as well as centre of gravity ($\mathrm{res} < 1.0\,\mathrm{mm}$). The structural model was updated based on results of a ground vibration test, so that the agreement between the experimental and the updated finite element modes is very good and all relevant modes are included. Good correlation was achieved for a frequency range of up to 15.0 Hz, which is more than sufficient for the intended aeroelastic applications. However, the combination of aerodynamics, structure, mass and flight mechanics can only be validated by flight test. In order to confirm that the manoeuvres sufficiently excite the structure and do not exceed the already mentioned 50 % of target load, all manoeuvrers described in section 4 were subject to a detailed loads analysis by introducing the control surface signals into the Loads Kernel software and performing a time-domain simulation. The results are visualised in Figure 9 as load envelopes.

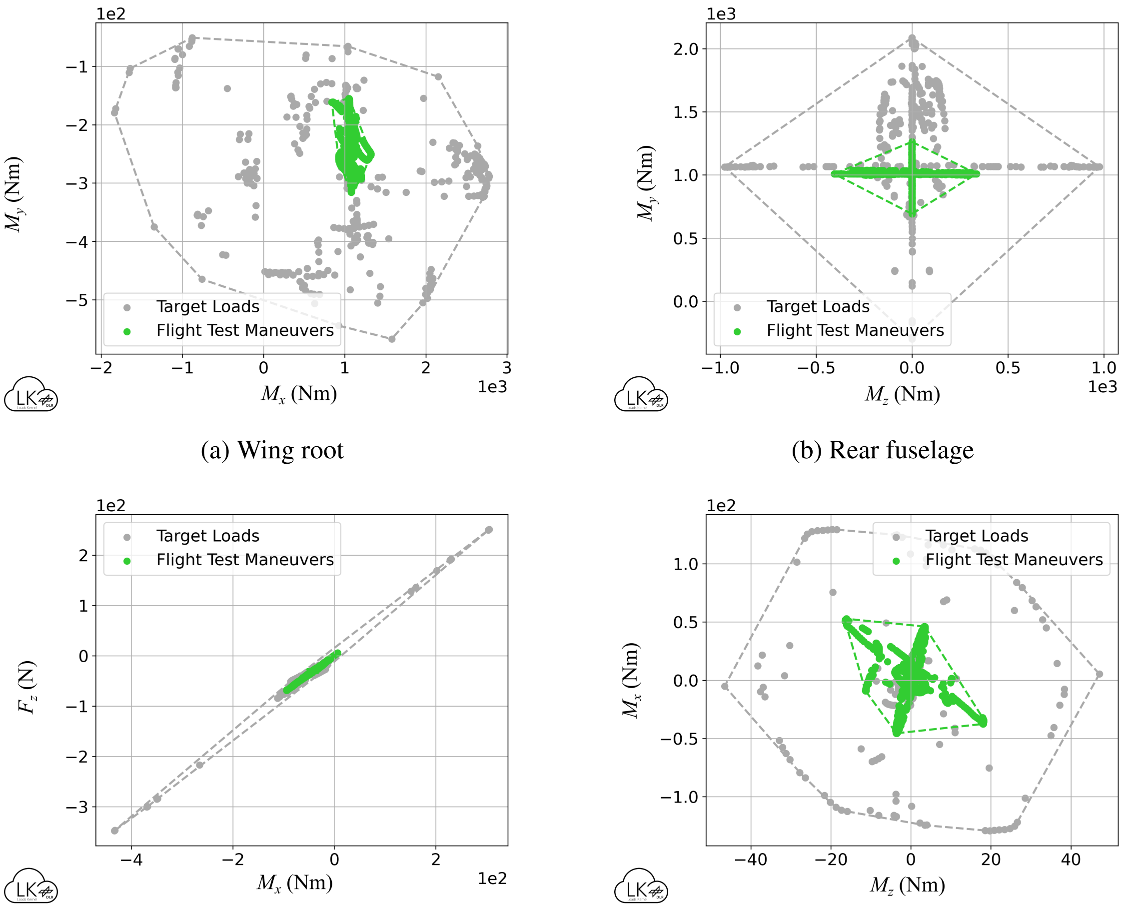

(a) Wing root (b) Rear fuselage

(c) Horizontal tail (d) Vertical tail

Figure 9: Load envelopes from flight test manoeuvrers compared to the target loads

Figure 9 shows two quantities of interest at four different monitoring stations, in Figure 9a for example the bending and torsional moments M_x and M_y at the right wing root. As a reference, the target loads used for the final sizing of the primary structure are shown in grey. It can be seen that in all four locations (Figure 9a - 9d), the loads due to the flight test manoeuvrers are well within the target loads. For the rolling and yawing manoeuvrers, the amplitude and duration of the control surface deflections were specifically designed and limited.

A deeper insight is given for the vertical manoeuvrers (Figure 10), were the top part of Figure 10a shows the stabiliser deflections i_{HTP} for three different vertical manoeuvrers, followed by the rigid body motion in terms of pitch rate q and Euler angle Θ. It can be seen that the inputs and the aircraft motion is pronounced. However, the load factor in vertical direction remains between $n_z = 0.75 \ldots 1.25$, which is comparably low considering the aircraft is sized for $n_z = 2.0$. The reason is again, that both the amplitude and duration of the control surface deflections were specifically designed and limited. Here however, the aircraft velocity was the driving constraint. The bottom part shows the forward velocity component u and it can be seen that the operational velocity envelope is already left, with occurring values slightly smaller than $V_{\mathrm{O,min}}$ an slightly larger than $V_{\mathrm{O,max}}$. This means that higher self-provoked load factors are simply not achievable at low altitude. Nevertheless, as shown in Figure 10b, these vertical manoeuvrers still provide a clear and pronounced time signal e.g. comparing the wing root bending moments M_x to the initial value at $t = 0.0$ s from the horizontal level flight.

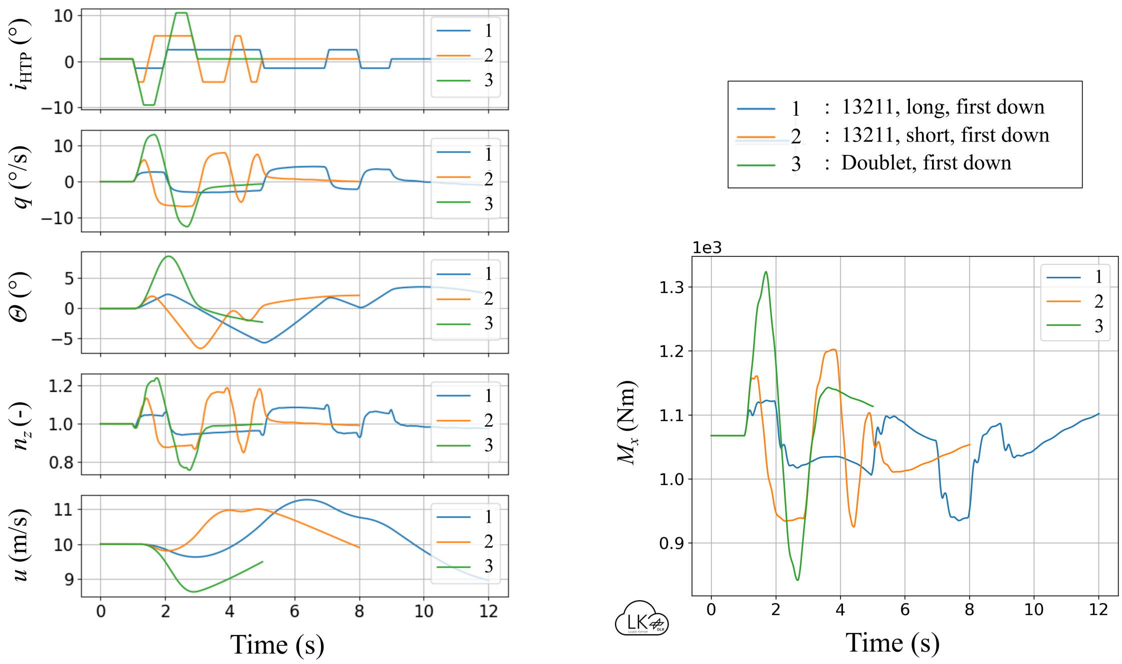

(a) Aircraft response

(b) Wing root bending moments

Figure 10: Time histories for vertical manoeuvres from dynamic aeroelasticity simulation

6 SYSTEM IDENTIFICATION TEST

The flight manoeuvres described in section 4 are designed to excite the aerodynamic and flexible dynamic characteristics of the HAP-alpha as effectively as possible while meeting the mentioned limiting requirements. The virtual flight data obtained from simulation of these manoeuvres will then be used in flight tests to determine the model parameters of the non-linear simulation model. Methods for system identification will be employed for this purpose. This section demonstrates the use of the manoeuvres for system identification. For the sake of simplicity, a linearised version of the HAP flight dynamic model is used.

6.1 Model Setup

A simplified model setup was employed to demonstrate the efficacy of the developed flight manoeuvrers for system identification. The non-linear flight dynamics model introduced in section 3 was linearised at a representative operating point, characterised by an altitude of 100 m and a true airspeed (V_{TAS}) of 10 m/s. The original model comprises 40 states, encompassing both rigid-body and flexible modes. However, for simplicity, the model was further reduced to include only the rigid-body modes and three flexible modes, resulting in a state vector $\vec{x}$ with 14 states. The linearised state-space model is represented by Eq. (6) and (7), which features the state vector $\vec{x}$, the input vector $\vec{u}$, and the output vector $\vec{y}$.

$$\dot{\vec{x}} = \underline{\underline{A}} \cdot \vec{x} + \underline{\underline{B}} \cdot \vec{u} \tag{6}$$

$$\vec{y} = \underline{\underline{C}} \cdot \vec{x} + \underline{\underline{D}} \cdot \vec{u} \tag{7}$$

The input vector u was also reduced to the stabiliser i_{HTP}, combined aileron $\hat{\xi}$ and rudder ζ deflection as inputs signals. The output vector $\vec{y}$ contains all the states and additionally the accelerations at centre of gravity in the body-fixed coordinate system a_x, a_z, a_y. This leads to a total of 17 outputs. The described model setup leads to the state-space matrices

$$\begin{aligned}
\underline{\underline{A}} &= \begin{bmatrix} a_{1,1} & a_{1,2} & \dots & a_{1,14} \\ a_{2,1} & a_{2,2} & \dots & a_{2,14} \\ \vdots & \vdots & \ddots & \vdots \\ a_{14,1} & a_{14,2} & \dots & a_{14,14} \end{bmatrix}, \quad \underline{\underline{B}} = \begin{bmatrix} b_{1,1} & b_{1,2} & b_{1,3} \\ b_{2,1} & b_{2,2} & b_{2,3} \\ \vdots & \vdots & \vdots \\ b_{14,1} & b_{14,2} & b_{14,3} \end{bmatrix}, \\
\underline{\underline{C}} &= \begin{bmatrix} c_{1,1} & c_{1,2} & \dots & c_{1,14} \\ c_{2,1} & c_{2,2} & \dots & c_{2,14} \\ \vdots & \vdots & \ddots & \vdots \\ c_{17,1} & c_{17,2} & \dots & c_{17,14} \end{bmatrix}, \quad \underline{\underline{D}} = \begin{bmatrix} d_{1,1} & d_{1,2} & d_{1,3} \\ d_{2,1} & d_{2,2} & d_{2,3} \\ \vdots & \vdots & \vdots \\ d_{17,1} & d_{17,2} & d_{17,3} \end{bmatrix}.
\end{aligned} \tag{8}$$

The state $\vec{x}$, input $\vec{u}$ and output vector $\vec{y}$ consist of the signals

$$\begin{aligned}
\vec{x} &= \begin{bmatrix} V_{\mathrm{TAS}} & \alpha & \beta & p & q & r & \Phi & \Theta & \eta_1 & \dot{\eta}_1 & \eta_2 & \dot{\eta}_2 & \eta_3 & \dot{\eta}_3 \end{bmatrix}^{\mathrm{T}}, \\
\vec{u} &= \begin{bmatrix} i_{\mathrm{HTP}} & \hat{\xi} & \zeta \end{bmatrix}^{\mathrm{T}}, \\
\vec{y} &= \begin{bmatrix} V_{TAS} & \alpha & \beta & p & q & r & \Phi & \Theta & \eta_1 & \dot{\eta}_1 & \eta_2 & \dot{\eta}_2 & \eta_3 & \dot{\eta}_3 & a_x & a_y & a_z \end{bmatrix}^{\mathrm{T}}.
\end{aligned} \tag{9}$$

The elements of the matrices $\underline{\underline{A}}$, $\underline{\underline{B}}$, $\underline{\underline{C}}$, and $\underline{\underline{D}}$ were initially obtained by a linearisation of the non-linear model. Therefore, for this investigation, it was necessary to introduce uncertainties to the model first. Consequently, 10 elements in matrix $\underline{\underline{A}}$, 6 elements in matrix $\underline{\underline{B}}$, and 4 elements in matrix $\underline{\underline{C}}$ were selected according to their expected influence on the rigid-body motion and altered. These modifications introduced errors of 50 % relative to the initial values, corresponding to either a 50 % increase or decrease. As the shapes of the flexible modes are assumed to be known, the introduced model errors were concentrated in the elements primarily affected by rigid-body motion and body accelerations in the output vector. Specifically, the following regions of the matrices in the state-space model were randomly modified:

- The first eight rows and columns of matrix $\underline{\underline{A}}$.
- The first eight complete rows of matrix $\underline{\underline{B}}$.
- The last three rows and first eight columns of matrix $\underline{\underline{C}}$.

The matrix $\underline{\underline{D}}$ of the state-space model remained unchanged. The modified model served as the basis for the subsequent system identification process.

6.2 Process Description

The absence of real flight data from the HAP-alpha aircraft necessitated the generation of virtual flight data for testing the system identification process. To this end, the non-linear flight dynamics model was used to simulate various flight manoeuvrers, with the trim point (altitude of 100 m, true airspeed V_{TAS} of 10 m/s) serving as the starting point. In order to introduce some measurement noise, a slight wind turbulence was introduced into the model input.

The simulated manoeuvres consisted of two short and long stabiliser 13211-manoeuvres to both sides, hence four altogether, two aileron 121-manoeuvres with different directions, and two short and long rudder doublets to both sides, i.e. four in sum. This set of manoeuvres will also be part of the first flight of the flight test campaign within *HAP-alpha*. In this system identification test, the frequency sweeps are excluded. This in in line with the flight test schedule of *HAP-alpha*. Since these manoeuvres are considered more critical, they will not be part of the first flight. Therefore, it is desirable that a system identification can be successfully performed using the remaining manoeuvres alone. Moreover, it is rather intended to excite the structural dynamics. In a first approach, this test run only addresses the rigid-body parameters.

In addition to the control deflections signals, all variables present in the output vector $\vec{y}$ of the linearised state-space model were included as measured variables. The MATLAB-based tool FITLAB [42], developed at the DLR Institute of Flight Systems, was employed to demonstrate the system identification process. This tool enables the direct import of a state-space model and the estimation of selected elements in the state-space matrices. The modified state-space model, as previously described, served as the basis for parameter estimation. Table 6 in the appendix lists all elements in the state-space matrices that were modified. The objective was to obtain new estimates of the selected modified elements in the state-space matrices. The maximum likelihood method was used to estimate the parameters, wherein the signals in the model output vector $\vec{y}$ were compared with the measurement vector $\vec{z}$. The parameters selected for estimation were determined through an iterative process, with the goal of minimising the model error or the difference between model output $\vec{y}$ and the measurement vector $\vec{z}$.

Using this parameter estimation process, the simulated flight test data were utilised to re-estimate the modified matrix elements. This approach simulates the process that will occur during real flight tests, where an existing model with known errors is improved using multiple system identification methods. By doing so, the effectiveness of the system identification process can be evaluated and refined prior to actual flight testing.

6.3 Results and Evaluation

The results of the system identification process are presented in the time series plots of Figure 11 to Figure 13. Please note that not all used manoeuvres are displayed here (cf. section 6.2). In Figure 11, the first plot depicts the stabiliser input. Subsequent plots in this figure show the longitudinal output vector quantities. The virtual flight data are represented by blue lines, while the response of the linear model with estimated state-space matrix elements is shown in red. Similarly, Figure 12 illustrates the signals for lateral aircraft motion. The first two plots display aileron and rudder deflections as model inputs, while the remaining plots compare lateral quantities from the simulated virtual flight test data (blue) against the linear model response (red). Figure 13 presents time series plots for the generalised-coordinate state variables of the first three flexible modes, again contrasting virtual flight test data (blue) with the linear model response (red).

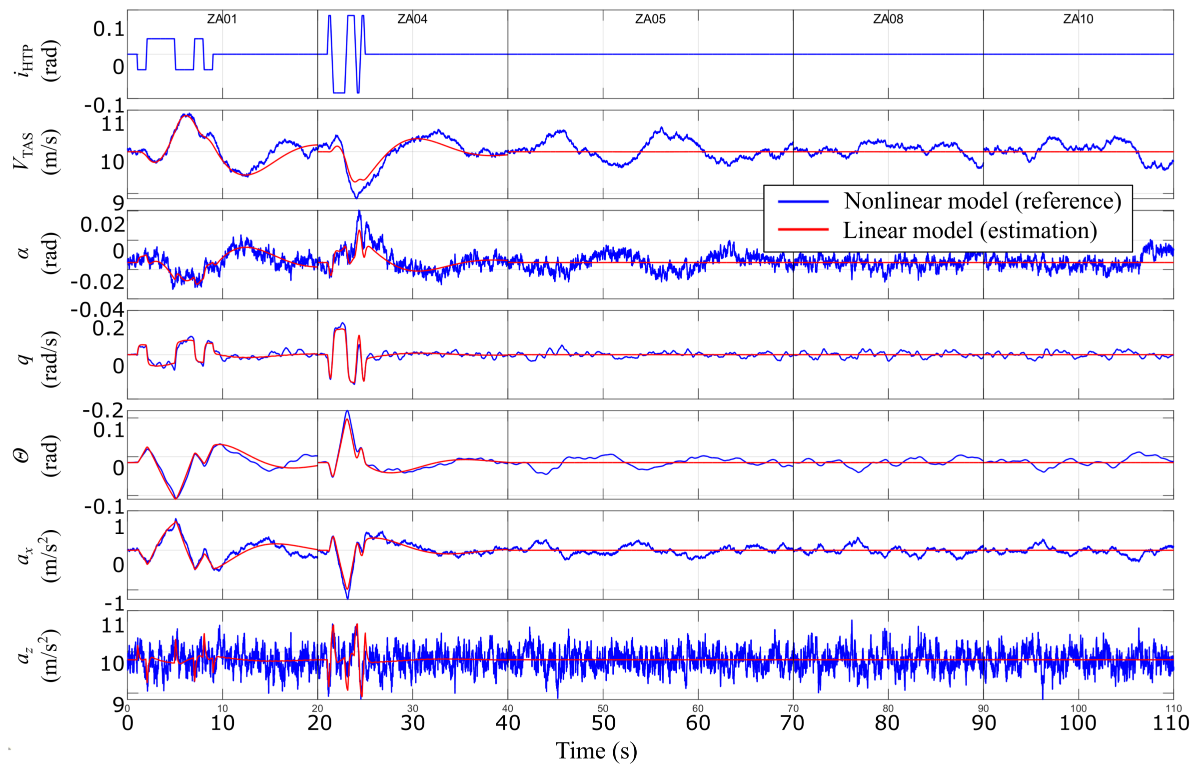

Figure 11: Longitudinal flight parameters from selected flight manoeuvrers, non-linear-model flight data as reference in blue, response of the linear flight model with estimated parameters in red

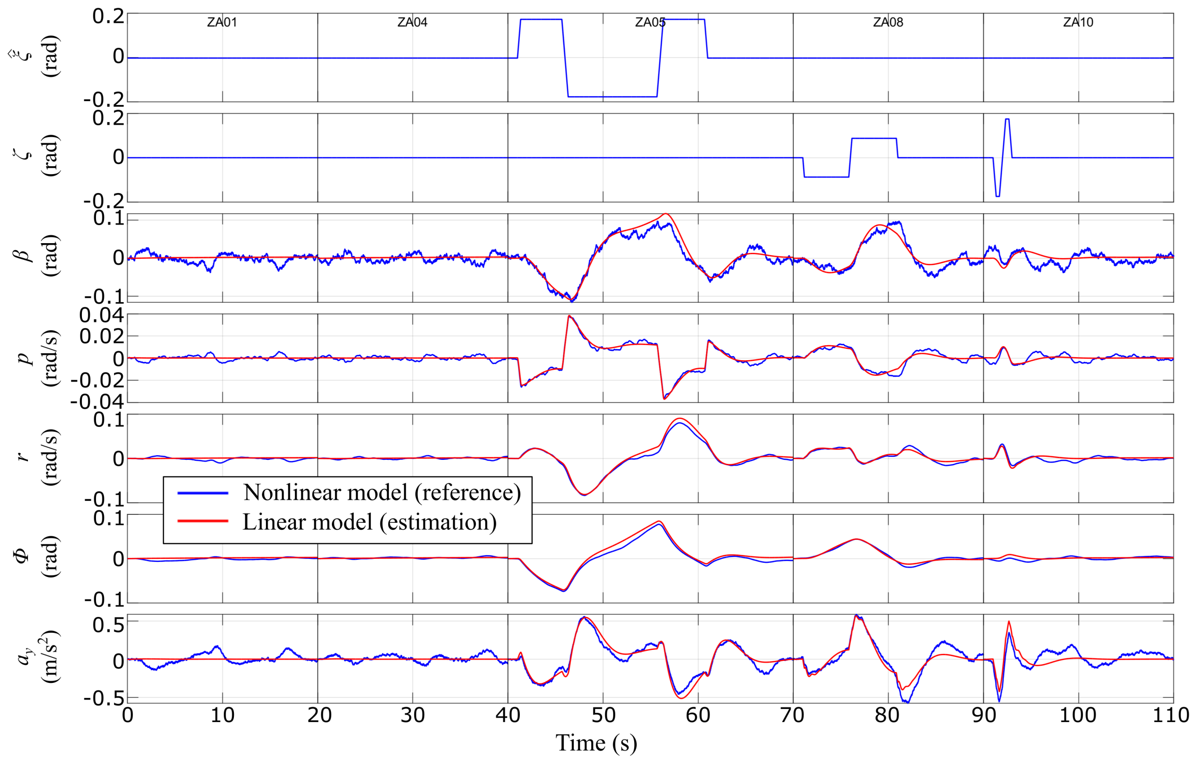

Figure 12: Lateral flight parameters from selected flight manoeuvrers, non-linear-model flight data as reference in blue, response of the linear flight model with estimated parameters in red

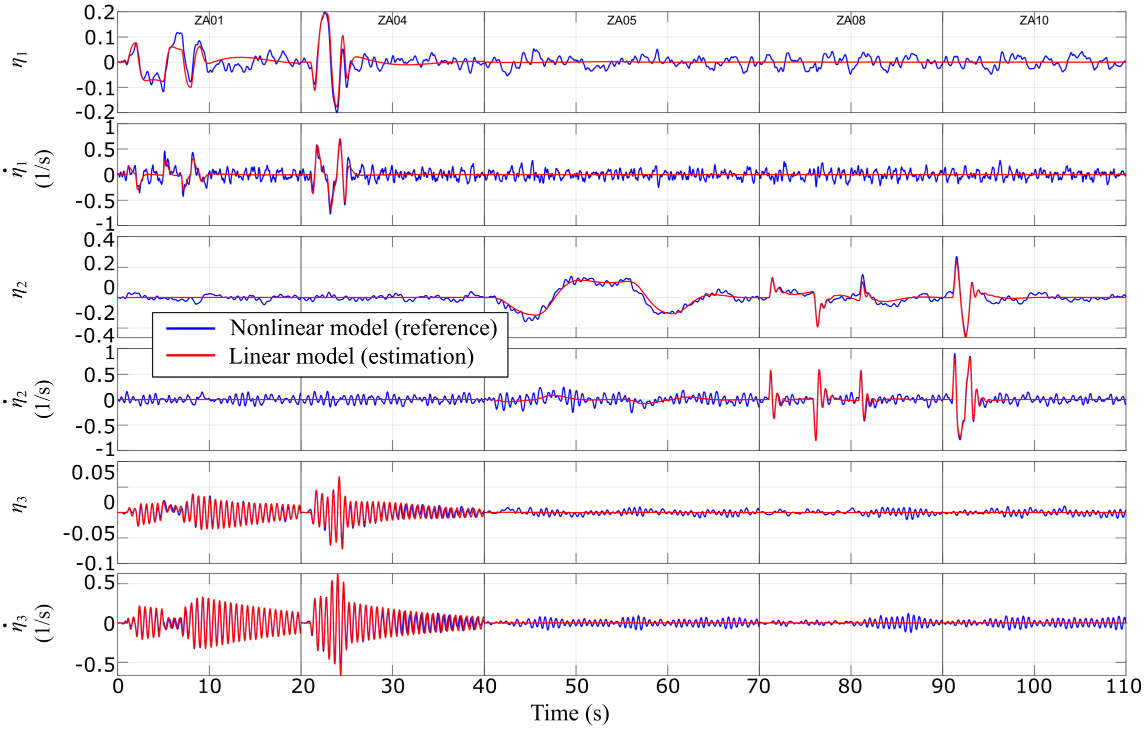

Figure 13: Flexible modes from selected flight manoeuvrers, non-linear-model flight data as reference in blue, response of the linear flight model with estimated parameters in red

In general, the virtual flight test data and the model output show good quantitative agreement for variables relating to rigid-body motion. This indicates that the linear model, utilizing the newly estimated elements in the state matrix, reproduces these variables effectively. In addition, the simulated measurements and linear model output for the first and second wing bending modes (η_1, $\dot{\eta}_1$, η_3, $\dot{\eta}_3$), as well as the first in-plane wing scissor mode (η_2, $\dot{\eta}_2$), are in close agreement.

Only minor deviations become apparent when considering the maxima and minima of V_{TAS}, angle of attack α, pitch rate q, pitch angle Θ, angle of sideslip β, yaw rate r and bank angle Φ. It is visible that the wind disturbances also lead to noticeable excitations but do not hinder the identification process. The results of the estimated parameters are provided in Table 6 in the appendix. This table lists the original, modified, and estimated values for the considered state-space matrices elements.

At this point, it should be noted that most of the parameters of the linear model reach an estimated value that is close to that of the initial linear model. However, this is not true for all cases, e.g. $\partial \dot{p}/\partial p$. At this point, it must be noted that the linear model, even though derived from the non-linear model, differs from it to a larger extent. There are multiple reasons for it. First, the non-linear model has a flight-shape dependency, which is lost in the linear model. This is especially important as the flight shapes, and with it the aerodynamic derivatives, already vary significantly between $V_{\mathrm{O,min}}$ and $V_{\mathrm{O,max}}$. Second, as the name says, the nonlinearities are lost, which is especially crucial for sideslip-angle-related effects at the VTP. Finally, most of the flexible states were excluded for simplicity in the linear model. The time histories of the estimated model demonstrate that the selected flight manoeuvres are, in principle, well-suited for identifying a simple linear flight dynamics model. The inclusion of further manoeuvres, such as frequency sweeps, will further improve the accuracy of the estimated model parameters.

FITLAB also enables the determination of parameters for a non-linear model. Therefore, in subsequent real-world flight tests with the HAP, the complete non-linear flight dynamics model will be incorporated into the system identification process.

7 CONCLUSIONS

This paper deals with the development of system identification manoeuvres for low-altitude flight testing of the DLR-aircraft HAP-alpha. For this purpose, different control surface signals are defined iteratively based on the time responses obtained by a flight dynamics simulation with the flexible aircraft. In addition, a loads analysis is performed and a final preliminary system identification test using a linear state-space model indicates that the manoeuvres are suitable for this purpose.

The HAP-alpha aircraft differs significantly from conventional aircraft, especially at low altitudes, in terms of its overcritically damped short period, and a strongly damped Dutch roll mode. Therefore, the sizing of test manoeuvres is different from the conventional approach, and cannot simply be performed using the natural frequencies of these modes. In addition, the roll performance of this aircraft is very low, which, together with a strong roll-yaw coupling, impedes the feasibility of typical bank-to-bank manoeuvres. Finally, the allowable airspeed band is very small and for reasons of risk mitigation, loads are required to be below 50 % of the target loads during these manoeuvres.

Taking all of these conditions into account, a set of manoeuvres is found that sufficiently excites all required rigid-body quantities and the aircraft's structural dynamics. These manoeuvres, in some part, differ notably from more typical manoeuvres. Three approaches are used to achieve this satisfactory set:

1. Strong adaptations of base durations and/or magnitudes: To obtain sufficient excursions related to strongly damped modes, either rather long inputs of small magnitude or very short inputs with high magnitudes are used.
2. Use of single manoeuvres twice with different parameters: In some cases, simultaneous pronounced excursions of steady and dynamic quantities are difficult to achieve. Here, the same manoeuvre can be applied twice with modified parameters, while shorter input sequences with stronger magnitude are used to increase the dynamic reaction and vice versa.
3. Use of less conventional types of input signals: In order to account for the aircraft's roll performance, different signals are used like a 121 and an aileron sine input.

Altogether, a short and a long 13211-manoeuvre, as well as a doublet manoeuvre using the stabiliser are found to yield satisfactory aircraft reactions in longitudinal motion. For roll, a longer 121 and an aileron sine input are defined and a short and a long rudder doublet are used to excite the yawing motion. Moreover, typical frequency sweeps are used about all axes, as these have shown to sufficiently excite the structural dynamics.

The final system identification test using a linearised model and simulation results from the non-linear model with light turbulence indicates that the manoeuvres are well applicable for system identification purposes. However, it must be mentioned that, at this point, only the flight quantities given at the centre of gravity were used and no sensor models along with measurement errors were included. To attenuate this simplification, only a small number of the manoeuvres were used for the identification test. Nevertheless, it must be admitted that the inclusion of sensors with their positions and errors will further complicate the identification and also aggravate the reconstruction of single modes. Particularly the signal-to-noise ratio is crucial with respect to the actual feasibility of the system identification. Therefore, the identification test performed in this paper serves to provide an idea about the general applicability of the found manoeuvres.

8 FUTURE WORK

As already described, the system identification test performed in this work is a first step that already gives an idea about the applicability of the developed flight test manoeuvres. The next step is to include sensor models with measurement errors and to repeat the analyses to consolidate the findings of this work. Moreover, the flight test campaign in the context of the project *HAP-alpha* is scheduled for summer 2026. The manoeuvres developed in this work will be performed within the campaign. The according flight test data will then be used for system identification and to validate and improve the available models.

ACKNOWLEDGEMENTS

The authors would like to thank the colleagues involved in the project *HAP-alpha*, particularly those who are part of the flight physics team and thereby contributed in setting up the flight dynamics model used in this work.

9 REFERENCES

[1] Airbus Defence and Space (2018). Airbus Zephyr, Solar High Altitude Pseudo-Satellite flies for longer than any other aircraft during its successful maiden flight. Press Release.

[2] Malewar, A. (2022). Airbus's solar-powered Zephyr UAS crashes after a 64-day flight. *Inceptive Mind*. Available online at `https://www.inceptivemind.com/airbus-solar-powered-zephyr-uav-crashes-64-day-flight/25969/` (Accessed: 2025-12-26).

[3] Runge, H., Rack, W., Ruiz-Leon, A., et al. (2007). A Solar Powered HALE-UAV for Arctic Research. *1st CEAS European Air and Space Conference*.

[4] Mohammed, A., Mehmood, A., Pavlidou, F.-N., et al. (2011). The Role of High-Altitude Platforms (HAPs) in the Global Wireless Connectivity. In *Proceedings of the IEEE*, vol. 99. pp. 1939–1953. doi:10.1109/JPROC.2011.2159690.

[5] Noll, T., Brown, J., Perez-Davis, W., et al. (2004). Investigation of the Helios Prototype Aircraft Mishap. NASA - Helios Mishap Investigation Board.

[6] National Transportation Safety Board (1st May 2015). Aviation Accident Report - Accident DCA15CA117. Titan Solara 50, N950TA.

[7] National Transportation Safety Board (28th June 2016). Aviation Accident Report - Accident DCA16CA197. Facebook Aquila, N565AQ.

[8] Australian Transport Safety Bureau (28th September 2019). In-flight break-up involving Airbus Zephyr unmanned aerial vehicle - AO-2019-056. Airbus Zephyr.

[9] Hasan, Y. J., Roeser, M. S., Hepperle, M., et al. (2022). Flight mechanical analysis of a solar-powered high-altitude platform. *CEAS Aeronautical Journal*. doi: 10.1007/s13272-022-00621-2.

[10] Hasan, Y. J., Fezans, N., and Voß, A. (2024). Flight Mechanical Analysis of a Very Flexible High-Altitude Platform Under Uncertainty Considerations. *34th Congress of the International Council of the Aeronautical Sciences*. ISSN 2958-4647.

[11] Nikodem, F. (2023). Overview of the DLR High Altitude Platform and Scientific Potential of the Technology Demonstrator HAP-alpha. *Deutscher Luft- und Raumfahrtkongress 2023*.

[12] Voß, A., Buchbach, R., Soal, K., et al. (2026). HAP-alpha: Model Updating Based on Ground Vibration Test and the Influence on Loads. *International Forum on Aeroelasticity and Structural Dynamics*. Submitted.

[13] Voß, A., Tang, M., and Sinske, J. (2026). Flight Test Instrumentation for Loads and Aeroelastic Analyses of a High Altitude, Long Endurance, Solar Electric Aircraft. *AIAA SciTech Forum 2026*. doi:10.2514/6.2026-1156.

[14] Hasan, Y. J., Roeser, M. S., and Voigt, A. (2022). Evaluation of the controllability of a remotely piloted high-altitude platform in atmospheric disturbances based on pilot-in-the-loop simulations. *CEAS Aeronautical Journal*. doi:10.1007/s13272-022-00626-x.

[15] Waszak, M. R. and Schmidt, D. K. (1988). Flight Dynamics of Aeroelastic Vehicles. *Journal of Aircraft*, 25(6), 563–571. doi:10.2514/3.45623.

[16] Plaetschke, E. and Schulz, G. (1979). Practical Input Signal Design. Tech. Rep. AGARD, Lecture Series No. 104, Paper 3, NATO.

[17] Jategaonkar, R. V. (2015). *Flight Vehicle System Identification - A Time Domain Merthodology: Second Edition*, vol. 245 of *Progress in Astronautics and Aeronautics*. Reston, VA, USA: AIAA. ISBN: 978-1-62410-278-3.

[18] Klein, V. and Morelli, E. A. (2006). *Aircraft System Identification: Theory and Practice*. AIAA education series. Reston, VA, USA: American Institute of Aeronautics and Astronautics. ISBN 9781563478321.

[19] Morelli, E. A. and Klein, V. (1990). Optimal input design for aircraft parameter estimation using dynamic programming principles. *Proceedings of the AIAA Atmospheric Flight Mechanics Conference*. doi:10.2514/6.1990-2801.

[20] Seren, C., Bommier, F., Verdier, L., et al. (2006). Optimal Experiment and Input Design for Flight Test Protocol Optimization. *Proceedings of the AIAA Atmospheric Flight Mechanics Conference and Exhibit*. doi:10.2514/6.2006-6280.

[21] Jauberthie, C. and Chanthery, E. (2013). Optimal input design for a nonlinear dynamical uncertain aerospace system. In *Proceedings of the 9th IFAC Symposium on Nonlinear Control Systems*, vol. 46, iss. 23. Elsevier, pp. 469 – 474. doi:10.3182/20130904-3-FR-2041.00060.

[22] Lichota, P., Szulczyk, J., Agudelo Norea, D., et al. (2017). Power spectrum optimization in the design of multisine manoeuvre for identification purposes. *Journal of Theoretical and Applied Mechanics*, 55(4), 1193–1203. ISSN 1429-2955. doi:10.15632/jtam-pl.55.4.1193.

[23] Hosseini, S., Göttlicher, C., and Holzapfel, F. (2019). Optimal input design for flight vehicle system identification via dynamic programming and the direct method for optimal control. *AIAA Scitech 2019 Forum*. doi:10.2514/6.2019-1319.

[24] Grauer, J. A. and Boucher, M. (2020). Aircraft System Identification from Multisine Inputs and Frequency Responses. *AIAA Scitech 2020 Forum*. doi:10.2514/6.2020-0287.

[25] Roeser, M. S. and Fezans, N. (2021). Method for designing multi-input system identification signals using a compact time-frequency representation. *CEAS Aeronautical Journal*. ISSN 1869-5590. doi:10.1007/s13272-021-00499-6.

[26] Koehler, R. and Wilhelm, K. (1977). Auslegung von Eingangssignalen für die Kennwertermittlung, DFVLR-IB 154-77/40. Tech. rep., DFVLR (today DLR), Braunschweig, Germany.

[27] Research and Technology Organization (2000). Flight Control Design – Best Practices, RTO-TR-029. Tech. rep., NATO, Neuilly-sur-Seine, Cedex, France.

[28] Plaetschke, E., Mulder, J., and Breeman, J. (1982). Flight Test Results of Five Input Signals for Aircraft Parameter Identification. *IFAC Proceedings Volumes*, 15(4), 1149–1154. ISSN 1474-6670. doi:10.1016/S1474-6670(17)63152-5. 6th IFAC Symposium on Identification and System Parameter Estimation, Washington USA, 7-11 June.

[29] Morelli, E. A. (1999). Flight test of optimal inputs and comparison with conventional inputs. *Journal of Aircraft*, 36(2), 389–397. doi:10.2514/2.2469.

[30] Fezans, N., Deiler, C., and Roeser, M. S. (2019). Generation of a Dataset for System Identification with VIRTTAC-Castor. *DLRK 2019*. doi:10.25967/490132.

[31] de Oliveira Silva, B. G. and Moennich, W. (2012). System Identification of Flexible Aircraft in Time Domain. *AIAA Atmospheric Flight Mechanics Conference*. doi:10.2514/6.2012-4412.

[32] de Oliveira Silva, B. G. (2018). *System Identification of Flexible Aircraft in Time Domain*. Phd thesis, Technische Universität Braunschweig, Braunschweig, Germany. DLR-FB-2018-29.

[33] Morelli, E. A. and Grauer, J. A. (2020). Practical Aspects of Frequency-Domain Approaches for Aircraft System Identification. *Journal of Aircraft*, 57(2), 268–291. doi:10.2514/1.C035599.

[34] Weiser, C., Schulz, S., Voß, A., et al. (2023). Attitude Control for High Altitude Long Endurance Aircraft Considering Structural Load Limits. *AIAA SciTech 2023 Forum*. doi:10.2514/6.2023-0106.

[35] Voß, A. (2020). Loads Kernel User Guide. Technical Report DLR-IB-AE-GO-2020-136, DLR Institute of Aeroelasticity, Göttingen, Germany.

[36] Voß, A. (2025). LoadsKernel Release 2025.01. Available online at `https://zenodo.org/records/14617118` [Accessed: 03-Feb-2025].

[37] Voß, A., Handojo, V., Weiser, C., et al. (2020). Preparation of Loads and Aeroelastic Analyses of a High Altitude, Long Endurance, Solar Electric Aircraft. *AEC2020 Aerospace Europe Conference*.

[38] Voß, A., Handojo, V., Weiser, C., et al. (January 2022). Results from Loads and Aeroelastic Analyses of a High Altitude, Long Endurance, Solar Electric Aircraft. *Journal of Aeroelasticity and Structural Dynamics*, 9. doi:10.3293/asdj.2021.58.

[39] Voß, A., Koch, C., Niemann, S., et al. (2022). Transition from Preliminary to Detailed Design of a Highly Elastic Solar Electric Aircraft. *International Forum on Aeroelasticity and Structural Dynamics*.

[40] Voß, A. (2020). An Implementation of the Vortex Lattice and the Doublet Lattice Method. Technical report dlr-ib-ae-go-2020-137, DLR Institute of Aeroelasticity, Göttingen, Germany.

[41] Voß, A. (2024). PanelAero Release 2024.02. Available online at `https://zenodo.org/doi/10.5281/zenodo.8343766` [Accessed: 13-Feb-2024].

[42] Seher-Weiß, S. (2024). FitlabGui - A MATLAB® Tool for Flight Data Analysis and Parameter Estimation, Updated Version of IB 111-2015/34.

COPYRIGHT STATEMENT

APPENDIX

Table 6: Results of parameter estimation

Parameter		Linear model	Initial mod. value	Estimated value	Standard deviation	Relative error
$a_{1,8}$	$\partial\dot{V}_{\mathrm{TAS}}/\partial\Theta$	-9.8125	-14.7187	-8.1235	0.0375	0.46 %
$a_{2,5}$	$\partial\dot{\alpha}/\partial q$	-0.1196	-0.0598	0.4049	0.0120	2.97 %
$a_{3,4}$	$\partial\dot{\beta}/\partial p$	-0.6784	-0.3392	-0.6415	0.0055	0.86 %
$a_{3,6}$	$\partial\dot{\beta}/\partial r$	-0.6468	-0.9702	-0.6709	0.0022	0.32 %
$a_{4,3}$	$\partial\dot{p}/\partial\beta$	-2.7405	-1.3702	-3.9119	0.1230	3.14 %
$a_{4,4}$	$\partial\dot{p}/\partial p$	-14.3473	-21.5209	-21.0412	0.6793	3.23 %
$a_{4,6}$	$\partial\dot{p}/\partial r$	3.0767	1.5384	4.1437	0.1285	3.10 %
$a_{5,2}$	$\partial\dot{q}/\partial\alpha$	-8.7079	-4.3540	-11.9881	0.0681	0.57 %
$a_{6,4}$	$\partial\dot{r}/\partial p$	-0.9006	-1.3509	-0.8866	0.0067	0.75 %
$a_{6,6}$	$\partial\dot{r}/\partial r$	-0.4891	-0.7337	-0.4787	0.0014	0.29 %
$b_{2,1}$	$\partial\dot{\alpha}/\partial i_{\mathrm{HTP}}$	-1.1638	-1.7457	-0.4832	0.0162	3.34 %
$b_{4,2}$	$\partial\dot{p}/\partial\hat{\xi}$	-1.0721	-1.6081	-3.0840	0.0980	3.18 %
$b_{4,3}$	$\partial\dot{p}/\partial\zeta$	0.0400	0.0200	0.1311	0.0101	7.67 %
$b_{5,1}$	$\partial\dot{q}/\partial i_{\mathrm{HTP}}$	-14.7876	-22.1814	-13.5980	0.0247	0.18 %
$b_{6,2}$	$\partial\dot{r}/\partial\hat{\xi}$	-0.0012	-0.0018	0.0088	0.0007	7.83 %
$b_{6,3}$	$\partial\dot{r}/\partial\zeta$	-0.3859	-0.1929	-0.3755	0.0011	0.30 %
$c_{15,8}$	$\partial a_x/\partial\Theta$	-9.8114	-14.7170	-9.4833	0.0450	0.47 %
$c_{16,3}$	$\partial a_y/\partial\beta$	-4.4762	-2.2381	-4.3482	0.0143	0.33 %
$c_{17,1}$	$\partial a_z/\partial V_{\mathrm{TAS}}$	-1.9530	-0.9765	-1.9294	0.0205	1.06 %
$c_{17,2}$	$\partial a_z/\partial\alpha$	-100.82	-151.23	-106.63	1.1122	1.04 %